BioNanoScience
https://doi.org/10.1007/s12668-024-01393-1

RESEARCH

Antimicrobial Properties and Cytotoxicity of Iron Oxide Nanoparticles Synthesized Using *Melia azedarach* Leaf Extract Against Diarrhoeal Pathogens

Tesleem Olatunde Abolarinwa[1,4] · Daniel Jesuwenu Ajose[1,4] · Bukola Opeyemi Oluwarinde[1,4] · Kotsoana Peter Montso[1,4] · Justine Fri[1] · Omolola Esther Fayemi[2] · Adeyemi Oladapo Aremu[3] · Collins Njie Ateba[1,4]

Accepted: 3 April 2024

Abstract

The high mortality and morbidity resulting from an increasing incidence of antibiotic resistance among pathogens highlight a crucial need for the development of novel alternative therapy. In the quest for alternative therapy, this study was conducted to synthesise nanoparticles (NPs) from ferric chloride hexahydrate ($FeCl_3.6H_2O$) via *Melia azedarach* L. (Meliaceae) leaf extract and evaluate their antibacterial properties against multidrug resistant pathogenic *Escherichia coli, Salmonella enterica,* and *Vibrio cholerae*. Multidrug-resistant pathogenic bacteria were isolated from cattle faeces and characterised by whole genome sequence analysis. The extracts from *M. azedarach* leaves were used as reducing, capping, and stabilising agents on the precursor metal ($FeCl_3.6H_2O$) to produce NPs. The biosynthesised NPs were characterised by ultraviolent visible (UV–vis) spectroscopy, X-ray diffraction (XRD), Fourier transform infrared spectrophotometry (FTIR), scanning electron microscopy (SEM), and transmission electron microscopy (TEM). The NPs were tested against multidrug-resistant bacteria to determine the minimum inhibitory concentration (MIC), minimum bactericidal concentration (MBC), and rate of kill. In this study, WGS analysis confirmed the bacteria (*E. coli*, *V. cholerae,* and *S. enterica*) isolates to be multidrug-resistant pathogen and NP that has a spherical shape with an average particle size of 49.75 nm was successfully biosynthesised. The NPs displayed significant antimicrobial activities with MIC of 62, 31, and 62 mg/mL, MBC of 500, 250, and 500 µg/mL, and the lowest killing times of 4, 2, and 3 h against *E. coli, V. cholerae,* and *S. enterica*, respectively. Interestingly, the concentrations of the NPs required to inhibit the growth of *E. coli*, *V. cholerae,* and *S. enterica* were not toxic to HEK293 cells. Based on the promising antimicrobial activities of the biosynthesised NPs in this study, they could be useful in important therapeutic applications aimed at combating multidrug-resistant pathogens.

Keywords Antimicrobial-resistance · Diarrhoea · Nanoparticles · Multidrug-resistance · Nanotechnology · Pathogen

✉ Collins Njie Ateba
collins.ateba@nwu.ac.za

[1] Antimicrobial Resistance and Phage Biocontrol Research Group, Department of Microbiology, School of Biological Sciences, Faculty of Natural and Agricultural Sciences, North-West University, Private Bag X2046, Mmabatho 2735, South Africa

[2] Department of Chemistry, Faculty of Natural and Agricultural Sciences, North-West University, Private Bag X2046, Mmabatho 2735, South Africa

[3] Indigenous Knowledge Systems Centre, Faculty of Natural and Agricultural Sciences, North-West University, Private Bag X2046, Mmabatho 2735, South Africa

[4] Food Security and Safety Niche Area, Faculty of Natural and Agricultural Sciences, North-West University, Private Bag X2046, Mmabatho 2735, South Africa

Abbreviations

AMR	Antimicrobial resistance
DNA	Deoxyribonucleic acid
DMEM	Dulbeco's modified eagle's medium
DMSO	Dimethyl sulfoxide
EMB	Eosin methylene blue
$FeCl_3.6H_2O$	Ferric chloride hexahydrate
FTIR	Fourier transform infra–red
HEK293	Human embryonic kidney 293
MBC	Minimum bactericidal concentration
MIC	Minimum inhibitory concentration
NP	Nanoparticle
PGAP	Prokaryotic genome annotation pipeline
RAST	Rapid annotation using the subsystem technology
RGI	Resistance gene identifier

Published online: 11 April 2024

SSA	Salmonella shigella agar
SEM	Scanning electron microscopy
TCBS	Thiosulfate citrate bile sucrose
TTC	Triphenyl tetrazolium chloride
TEM	Transmission electron microscopy
UV–vis	Ultraviolent visible
WGS	Whole genome sequencing
XRD	X-ray diffraction

1 Introduction

Diarrhoea is among the most frequent causes of illness and fatality, even in a country with an advanced healthcare facility [1]. The impact of diarrhoea is aggravated by the ever-increasing incidence of antimicrobial resistance (AMR) among the causative agents. This is now categorized as a public health challenge [2]. The AMR among diarrhoeagenic pathogens also contributes to treatment failure, huge economic losses, and extended infection duration, even in a country with advanced public health policies and facilities [3, 4]. Also, administration of antibiotics is contraindicated for diarrhoea caused by some strains of bacteria, such as *E. coli* serotype O157 [5–7]. In addition, there is evidence that antibiotics might aggravate the risk of developing more life-threatening complications including hemorrhagic colitis, haemolytic uremic syndrome, and thrombotic thrombocytopenic purpura which account for a large number of cases of kidney failure [6, 8, 9]. According to the estimate of the global burden of disease in 2019, diarrhoea was the 3rd and 5th leading causes of morbidity in children below five years of age and all ages, respectively [3, 10].

The increasing incidence of AMR and contraindications associated with the administration of antibiotics limit the usage of antibiotics, most especially in diarrhoeal cases. This emphasizes the crucial need for the expansion of innovative strategies aimed at combating infections, controlling the development of antibiotic resistance, and spread.

Nanoparticles are particles that have a size ranging from 1 to 100 nm and possess a wide surface area to volume ratio. The smaller size and wider surface area to volume ratio enhance their physicochemical properties, making them suitable antimicrobial agents [11]. They are made of organic material, metal oxide, carbon, or metal [12]. Findings from several studies have reported the high efficacy of various metal NPs against a variety of multidrug-resistant pathogenic bacteria [13]. However, the development of various side effects, including argyrosis, argyria, liver damage, kidney obstruction, and eye irritation, in patients limits the usage of metal NPs for oral treatment of drug-resistant bacteria in human medicine [14]. This necessitates the need to choose the most promising metal candidate in terms of cost, environmental, and health biocompatibility when synthesising NPs from metal for medicinal use. Due to their biocompatibility, antibacterial efficacy, non-toxic and life sustainability, NPs produced from health-essential metals such as iron have been proven to be promising candidates for oral therapy in the field of medicine. NPs derived from iron metal are safe for oral therapy since they are part of the essential metals required by the body for life sustainability [15].

Three different techniques, namely chemical, physical, or biological methods, can be utilised in the synthesis of metal NPs [16]. However, the utilisation of expensive equipment, high energy consumption, low material conversion, and the generation of toxic waste from the chemical reducing agents employed in the physical and chemical processes limit their usage [17]. As a result of these limitations, most studies typically concentrate on biological synthetic techniques [11, 18, 19]. Biological synthetic methods are less expensive, easier to carry out, safer, more ecologically friendly, biocompatible, and have a wider range of applications compared to traditional physical and chemical approaches [11, 20]. In the biological method of synthesis, plant-mediated synthesis is the most preferred method as a result of its numerous advantages [20]. This is because plants are cheap, readily available in abundance, not harmful in most cases, eco-friendly, bio-compatible, and non-pathogenic, among others [11, 20].

Melia azedarach L. is among the plants that have been confirmed to contain phytochemicals (alkanoids, flavonoids, phenols, and tannins) that can reduce metal salts to NPs [21]. Due to their small size and wide surface area to volume ratio, NPs can simultaneously attack target cell constituents such as proteins, DNA, enzymes, and the cell membrane, leading to cell damage or death [2]. The potential of NPs to concurrently target multiple biomolecules can make it very difficult for pathogenic organisms to develop resistance against these antibacterial agents.

This study was designed to produce NPs from $FeCl_3.6H_2O$ mediated via *M. azedarach* leaf extract and assess their antimicrobial activities against multidrug-resistant *E. coli, S. enterica,* and *V. cholerae*.

2 Materials and Methods

The aseptic technique was fully implemented in this study. Ferric chloride hexahydrate ($FeCl_3.6H_2O$) purchased from Labchem (South Africa) was used as the metal salt precursor in the synthesis of NPs. Culture media (nutrient broth, nutrient agar, and Mueller–Hinton agar) were purchased from Neogen Laboratory (Heywood, UK). Analytical grade water from a Millipore Milli-Q gradient filtration system (Millipore, USA) was utilised throughout the experiments.

2.1 Ethics Approval

The ethics clearance for the study was collected from the North-West University (NWU) AnimCare Committee, and an ethics number of NWU-00771–23-A5 was assigned to this study.

2.2 Isolation of Bacteria from Cattle Faeces

Faecal samples were collected directly from the rectum of cattle and cultured on Eosin methylene blue (EMB) agar, Salmonella shigella agar (SSA), and Thiosulfate citrate bile sucrose (TCBS) agar, respectively. The plates were inverted and incubated aerobically at 37 ℃ for 24 h. The colonies with a green metallic sheen were selected on EMB agar for presumptive *E. coli*. Transparent or colourless colonies with or without a black centre were selected on SSA for presumptive *Salmonella* species. Yellowish colonies were selected on TCBS agar for presumptive *Vibrio* species.

All the presumptive isolates were tested against eight (8) panels of antibiotics belonging to different categories of antimicrobial agents accomplished by the disk diffusion method in accordance with clinical and laboratory standards institute guidelines [22]. The tested antibiotics were azithromycin, imipenem, levofloxacin, penicillin, streptomycin, sulfamethoxazole, tetracycline, and vancomycin.

Genomic deoxyribonucleic acid (DNA) was extracted from overnight cultures of the three selected multidrug-resistant presumptive bacterial isolates (one *E. coli,* one *Salmonella* species, and one *Vibrio* species) using a Zymo research genomic DNA^{TM} tissue miniprep kit (Zymo Research Corp, Irvine, CA, USA) following the manufacturer's instructions. The extracted DNA samples were subjected to WGS, and the raw read sequence was uploaded to the Kbase online platform version 2.1 (https://kbase.us/) for assembly and annotation. The annotated sequences were submitted to the GenBank for accession numbers.

The taxonomy of the isolates was generated by uploading sequences to the genomic taxonomy database (https://narrative.kbase.us/#appcatalog/app/kb_gtdbtk/run_kb_gtdbtk_classify_wf/release) on Kbase. The group in which the isolates belong, based on pathogenicity, was determined by searching the specific isolate contigs against the PathogenFinder version 1.1 database (https://cge.food.dtu.dk/services/SerotypeFinder/) on the genomic epidemiology online platform (https://www.genomicepidemiology.org/services/). The detection of the virulence genes harboured by the isolates was assessed by searching their contigs against the VirulenceFinder version 2.0 database (https://cge.food.dtu.dk/services/VirulenceFinder/). The AMR gene harboured by the isolates was predicted by uploading the contigs to the online resistance gene identifier (RGI) platform (https://card.mcmaster.ca/analyze/rgi).

2.3 Collection and Preparation of Plant Extract

Ten (10) kg of *M. azedarach* healthy leaves was obtained from Unit 2 in Mafikeng, North-West Province, South Africa. A voucher specimen (ATO2) was deposited at the S.D. Phalatse Herbarium, Department of Botany, North-West University, Mafikeng Campus, South Africa. The leaves were rinsed with sterile distilled water to remove dust particles, dried, and ground into a fine powder. About 100 mL of sterile distilled water was added to 5 g of the powder sample and vortexed to form a solution. The solution was boiled for 24 h at 60 °C inside a shaking incubator. Thereafter, the solution was filtered through Whatman filter paper to obtain the extract. The phytochemical screening of the extract was done following the methods described by Shubham et al. [23].

2.4 Synthesis of Iron Oxide Nanoparticles

In the preparation of the NPs, $FeCl_3.6H_2O$ was utilised as an iron precursor metal salt and extract from *M. azedarach* leaves as reducing, capping, and stabilising agents. The NPs were prepared by adding a 0.1 M $FeCl_3$ solution to extracts of *M. azedarach* leaves in a volume ratio of 1:1. The mixture was stirred for 60 min and then allowed to stand at room temperature for another 30 min. The colloidal suspension obtained was centrifuged, washed several times with ethanol, and then dried at 40 °C under vacuum to obtain pure NP (Fig. 1).

2.5 Characterisation of Synthesised Nanoparticles

The synthesised NPs were characterised by X-ray diffraction spectrophotometer (D8 Advance with DAVINCI design), scanning electron microscopy (Zeiss Ultra Plus 55 HRSEM, Germany), transmission electron microscopy (JEOLJEM 2100 electron microscope, JOEL ltd, TYO, Japan), UV–vis spectrophotometer (Agilent Technology, Cary series), and Fourier transformed infrared spectrometer (Agilent Technology, Carry 600 series FTIR spectrometer).

2.6 Preparation of Nanoparticle Suspensions

The NP suspension was prepared by adding 1000 µg of NPs to 1 ML of dimethyl sulfoxide (DMSO). The mixture was allowed to sonicate for 30 min to form a solution. The solutions were filter sterilized using 22 nm microfuge filters.

2.7 Preparation of Bacterial Inoculum

Prior to the antimicrobial test, *E. coli, V. cholerae,* and *S. enterica* were revived in nutrient broth and incubated aerobically at 37 ℃ for 24 h. The absorbance of the bacterial

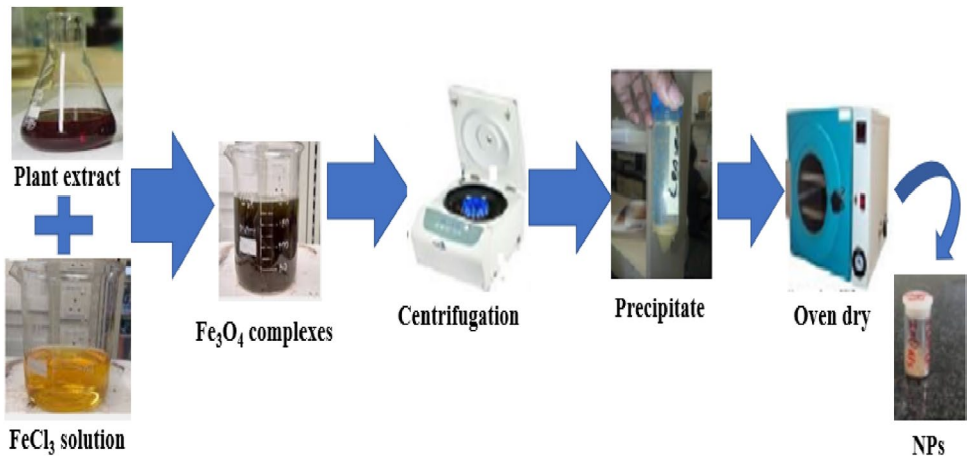

Fig. 1 Schematic representation of the synthesis of nanoparticles mediated by plant extracts

cultures was standardized using a spectrophotometer (Model MB-580, Shenhen Huisong Technology Development Co., Ltd., Shenzhen, China) at 600 nm to attain a viable cell count of 1.5×10^7 CFU/mL (optical density of 0.5).

2.8 Antibacterial Activities of the Nanoparticles

The sensitivity of diarrhoeagenic bacteria to synthesised NP was determined using a 2,3,5 triphenyl tetrazolium chloride (TTC) assay. The TTC test serves as an indicator system for the determination of the viability of the bacterial cell. The test relies on hydrogen ions released by dehydrogenase enzymes, which subsequently reduce the colourless tetrazolium salt to a red compound called formazan. The viable bacteria will change the colour of the TTC solution to red, while the dead cells will remain colourless. Firstly, all microtiter plate wells marked for the experiments were filled with 100 µL of NP solution. Subsequently, 100 µL of 18-h-old diarrhoeagenic bacterial isolates of 0.5 McFarland standardized was aseptically added to each well, mixed, and incubated at 37 ℃ for 24 h. The DMSO was utilised as a solvent control. After 24 h of incubation, 20 µL of the 1% tetrazolium salt solution was added to each well and further incubated for 1 h. The experiment was carried out in triplicate.

2.9 Minimum Inhibitory Concentration

The minimum inhibitory concentration (MIC) is the lowest concentration of antimicrobial agent needed to stop the growth of microorganisms. The MIC of the NPs was determined using 96-well microplate broth dilution method and TTC as an indicator reagent. Firstly, all the microtiter plate wells marked for the experiment were filled with 100 µL of DMSO. Exactly, 100 µL (1000 µg /mL) of NP solution was added to the first well and dilution was carried out to obtain different concentrations (500, 250, 125, 62, 31, 16, and 8 µg/mL) of NP. Subsequently, exactly 100 µL of the standardized bacteria isolate was aseptically added to each well and incubated at 37 °C for 24 h. The DMSO was added to the experiment as solvent (negative) control. After 24 h of incubation, 20 µL of the 1% tetrazolium salt solution was added to each well and further incubated for 1 h. The plates were then observed for colour change, and the MIC of NPs was taken as the lowest concentration of the NPs with no change in colour. The experiment was carried out in triplicate.

2.10 The Minimum Bactericidal Concentration (MBC)

The minimum bactericidal concentration (MBC) is the lowest concentration of the antimicrobial agent needed to kill microorganisms tested. The MBCs of the plant-derived nanoparticles against tested *E. coli, V. cholerae,* and *S. enterica* were determined from the MIC experiment. Immediately the MIC was determined, the wells that contained MIC and above concentration suspension were marked. Exactly 100 µL of the suspension from each marked well was withdrawn and mixed with molten nutrient agar at 45 ℃ and poured into the Petri plates. The plates were then incubated at 37 ℃ for 24 h and colony formation was observed. The MBC was taken as the lowest concentration of the NPs with no colony formation.

2.11 Time-Kill Assay

The antimicrobial efficacy test commonly termed time-kill assay is used to determine the bacterial activity of an antimicrobial agent over time. To determine the time of kill, firstly, all the microtiter plate wells marked for the experiments were aseptically filled with 100 µL of standardized bacterial isolate. Thereafter, 100 µL of NP solution at MBC was introduced to the wells. The killing rate was determined for

24 h (0, 2, 4, 6, 8, 10, 12, 14, 16, 18, 20, 22, and 24 h) at 37 ℃. The DMSO was used as a solvent control.

To determine the viability of the tested bacteria after NP treatment, 100 µL of suspension was withdrawn in time intervals (0, 2, 4, 6, 8, 10, 12, 14, 16, 18, 20, 22, and 24 h) mixed with molten nutrient agar at 45 ℃ inside petri dish. The plates were then incubated at 37 ℃ for 24 h. The colonies were counted and expressed as a colony-forming unit per millilitre (CFU/mL).

2.12 Toxicity Assay of Plant-Derived Nanoparticles

Cytotoxicity is how toxic a substance is to the cells and the kidney is an effective organ that removes waste and toxic substances from the body. In this study, human embryonic kidney 293 (HEK293) cells were used for the cytotoxicity test. Also, the trypan blue exclusion test described by Strober (2015) was used to detect the toxicity of the NPs to the cell (HEK293) after being treated with the NPs at different concentrations.

Prior to the NP cytotoxicity test, the HEK293 cell lines were grown in a high glucose medium called dulbeco's modified eagle's medium (DMEM) with a pH of 7.2. The DMEM was supplement with 10% foetal bovine serum, 100 µg/mL of streptomycin and 100 µg/mL penicillin. The cell lines were indirectly stained with Hoechst 33,258 to confirm that it is mycoplasma-free. The confirmed mycoplasma-free cell lines were used in this study within three months of thawing the frozen stock.

Firstly, cells line (HEK293) were seeded into a 96-well microtitre plate containing 100 µL DMEM and incubated for 24 h at 37 ℃ in a 5% CO_2 humidified incubator. Thereafter, NPs at different concentrations (8, 16, 31, 62.5, 125, 250, and 500 µg/mL) were aseptically added and incubated further for 24 h. After, 20 µL of the incubated mixture was withdraw and added to 80 µL of trypan blue and observed under a binocular microscope. The DMSO was used as solvent (negative) control. The percentage of cell viability was calculated using the formula: %cell viability = (Number of viable cells / numbers of control viable cell) X 100.

3 Result and Discussion

3.1 Profile of Bacteria Isolated

A total of 569 bacteria were isolated from the 269 analysed faecal samples. Out of 569 bacteria isolated, 300 presumptive *E. coli,* 50 presumptive *Salmonella* species, and 67 presumptive *Vibrio* species were identified based on morphological characteristics. A large proportion (73, 100, and 60%) of the presumptive *E. coli, Salmonella* species, and *V. cholerae*, respectively, were multidrug resistant (Fig. 2).

Based on WGS analysis, the three isolates were confirmed as *Escherichia coli, Vibrio cholerae,* and *Salmonella enterica* with accession numbers CP121294, CP122254, and CP123007, respectively. The genomes of these three isolates harboured virulent genes such as those responsible for adherence, invasion, and toxin production (Table 1). In addition, the genomes carried antibiotic resistant genes, which confer resistance to drugs such as macrolide (*kpnF, kpnE, H-NS, CRP*), fluoroquinolone (*emrB, emrR, acrAB-TolC, marA, soxR, rsmA, H-NS, CRP*), aminoglycoside (*acrD, kdpE, baeS, cpxA, baeR, kpnE, kpnF*), carbapenem (*marA, soxS*), cephalosporin (*EC-13, acrE, acrS, marA, kpnE, kpnF, soxS,*

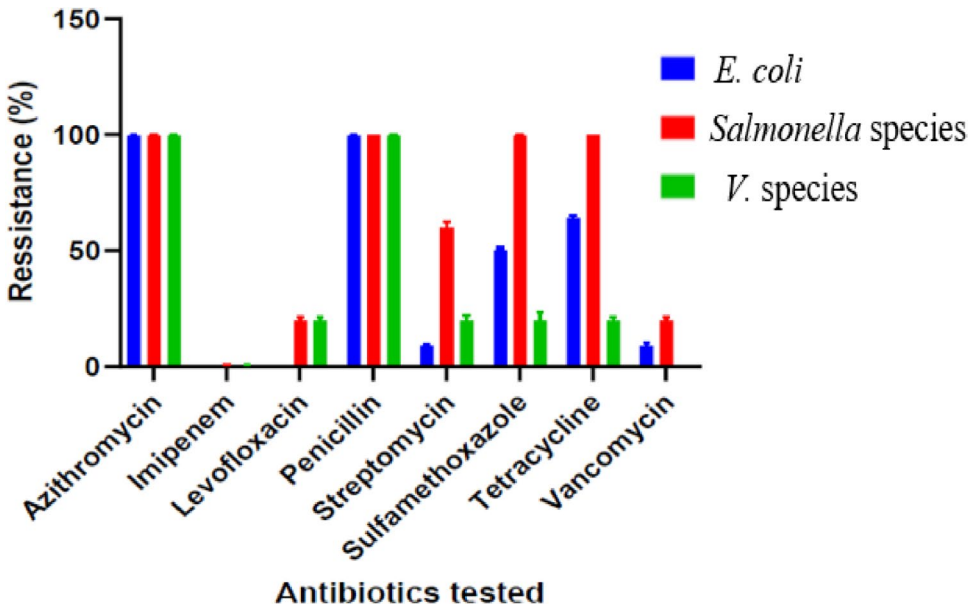

Fig. 2 Antibiotics resistance profile of isolated presumptive bacteria. The error bars represent standard deviations

Table 1 Virulence profile of the isolates

Escherichia coli		*Vibrio cholerae*		*Salmonella enterica*	
Virulence genes possessed by the isolates base on whole genome sequence analysis					
Virulence factor	**Related gene**	**Virulence factor**	**Related gene**	**Virulence factor**	**Related gene**
Virulence factor class (adherence)					
CFA/I fimbriae	*cfaA, cfaB, cfaC, cfaD*	Flagella L-ring protein	*fleR, flgC*	Afimbrial adhesin AFA-I	*afaB*
Curli fibres	*cgsA, cgsB, cgsC, cgsD*	Lateral flagella	*lafC, lafT, lfhA, nueA*	curlin major subunit CsgA	*csgA, csgB, csgC, csgD*
E. coli common pilus (ECP)	*acpA, acpB, acpC, acpD*	Flagellar motor switch protein	*fliM*	Bcf	*bcfA, bcfB, bcfC, bcfD*
E. coli laminin binding fimbriae	*elfA, elfC, elfD, elfG*	Flagellar biosynthesis protein	*fliP*	Type I fimbriae	*fimA, fimC, fimD, fimF*
Formate efflux transporter	*focC*			Stb	*stbA, stbB, stbC, stbD*
Hemorrhagic E. coli pilus (HCP)	*hcpA, hcpB, hcpC*			Std	*stdA, stdB, stdC*
P fimbriae	*papC*			Type IV pili	*pilQ, pilR, pilS, pilW*
Virulence factor class (iron uptake)					
Achromobactin biosynthesis and transport	*cbrD*	Periplasmic binding protein-dependent ABC transport sys	*viuC*	Outer membrane siderophore receptor	*iroN*
TonB-ExbBD energy transducing system	*tonB*	Iron/manganese transport	*sitA, sitB, sitC, sitD*	Aerobactin siderophore receptor	*iutA*
Putative regulatory protein	*yigQ*	Heme transport/ Heme uptake	*shuV/ chuA, chuS, chuU*	aerobactin biosynthesis protein	*iucD*
Virulence factor class (invasion)					
Invasion of brain endothelial cells	*ibeA, ibeB,* and *ibeC*	Flagella (Burkholderia)	*cheB, cheR, cheW, cheZ*	Signal transduction histidine-protein kinase	*barA*
Methyl-directed repair DNA adenine methylase	*dam*	Flagellar basal-body rod protein	*flgB*	Surface presentation of antigens protein	*spaR*
Phosphoethanolamine transferase	*yijP*			3-Phosphoshikimate 1-carboxyvinyl-transferase	*aroA*
UTP-glucose-1-phosphate transferase	*galU*			Cell invasion protein	*sipC*
Arylsulfatase	*aslA*			Salmonella invasin chaperone	*sicA*
Virulence factor class (secretion system)					
ACE T6SS	*aec31*and *aec32*	EPS type II secretion system	*epsE, epsG*	TTSS (SPI-1 encode)	*hilA, invA, orgA, orgB*
LEE locus encoded TTSS	*escV*	Flagella (cluster I)	*flgB, flgC, flgD, flgE, flgF, flgH*	TTSS (SPI-2 encode)	*ssaC, ssaD, ssaE, ssaG,*
				TTSS-1 translocated effectors	*avrA, sipA, sipB, sopB*
				TTSS-2 translocated effectors	*pipB, sopD2, sseF, sseJ*
Virulence factor class (toxin)					
Hemolysin/cytolysin A	*hlyE/clyA*	Heat-stable cytotonic/ enterotoxin	*Ast,*	SpvB	*spvB*
		Hemolysin HlyA	*hlyA*	Typhoid toxin	*cdtB, pltA*

H-NS), tetracycline (*acrA, sdiA, acrAB-TolC, marR, soxR, kpnF, kpnE*), peptide (*vanG*), aminocoumarin (*mtdA, mtdb, mtdC, baeS, cpxA, baeR*), rifamycin (*acrS, acrA, acrB, rsmA, mdtM, marA, soxS*), and phenicol (*acrA, sdiA, acrAB-TolC, marR, soxR, rsmA).*

3.2 Phytochemical Analysis

The phytochemical test of the *M. azedarach leaf* extract was carried out to determine its bioactive compounds. The confirmed phytochemicals were flavonoids, phenols, saponins and tannins. Several researchers have confirmed that these phytochemicals have a reducing, capping and stabilising capacity necessary for NP synthesis [21].

3.3 Synthesis of Nanoparticles

In this study, NP was synthesised using $FeCl_3.6H_2O$ as the iron precursor and extracts of *M. azedarach* leaves as reducing and stabilising agents. The formation of NPs was confirmed by the appearance of an intense black colour change upon the addition of the *M. azedarach* leaf extracts with brownish to light-yellow colour $FeCl_3.6H_2O$ solution. Similar results were reported by Madubuonu et al. [24], where a change to black colour was encountered with the addition of *Psidium guajava* extract to the yellow-coloured $FeCl_3.6H_2O$ precursor salt solution. In a study by Zambri et al. [25], the formation of Fe_3O_4-NPs was confirmed with the formation of a black precipitate on the addition of the neem leaf extract to the ferric chloride precursor. Change in colour signifies excitation of plasmon vibration from metal nanoparticles [26]. Chauhan and Upadhyay [27] reported the formation of a black precipitate on the addition of *Lawsonia inermis* leaf extract to $FeCl_3.6H_2O$ salt solutions within a few minutes.

3.4 Ultraviolet–Visible (UV) Spectroscopy

The confirmation of NP formation was accomplished by the UV–vis spectroscopy method with a wavelength range of 200–800 nm. UV shows an absorbance peak at 284 nm and strong absorption peak at 301 nm for the synthesised NPs (Fig. 3). This indicates the stability of the particles in the solution and the formation of Fe_3O_4-NPs. A similar spectrum was also observed in the study conducted by Aisida et al. [28], where an absorption peak of 305 nm was reported for Fe_3O_4-NPs. Neupane et al. [29] reported an absorption peak of 310 nm, from Fe_3O_4-NPs mediated by plant extracts. Moreover, the absorption peak maximum obtained was close to the observed UV spectrum range of 307 nm for Fe_3O_4-NPs reported by Rahman et al. [30].

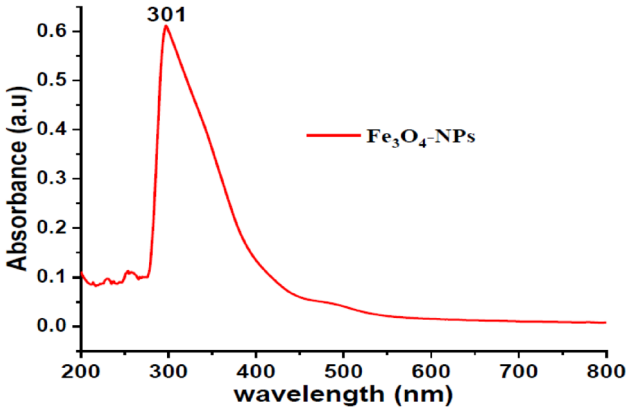

Fig. 3 Ultraviolet–visible spectrum of the iron oxide nanoparticles mediated via the extract of *Melia azedarach* leaves

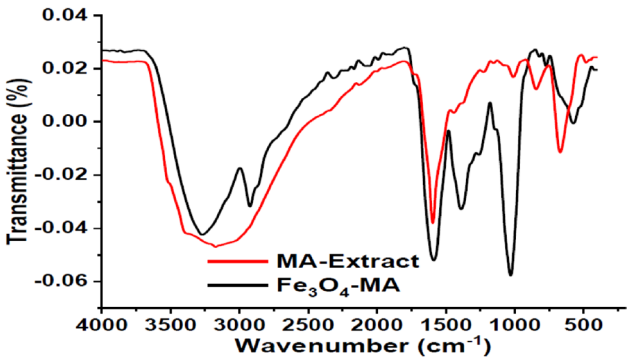

Fig. 4 Fourier transform infrared spectrum of iron oxide nanoparticles mediated by *Melia azedarach* (MA) leaves extract

3.5 Fourier Transform Infrared Spectroscopy (FTIR)

The FTIR analysis for this study was performed in the spectral range of 4000 to 400 cm^{-1}. From the study conducted, the IR spectra of the extracts of *M. azedarach* leaves and synthesised Fe_3O_4-NPs are shown in Fig. 4. A strong peak showing chemical structures for the extract of *M. azedarach* leaves was observed around 3273 cm^{-1}, which falls within the range of 3000–3700 cm^{-1}, confirms the presence of OH stretch. The confirmation of hydroxyl group indicates the present of flavonoids, polyphenols, and alcohol functional group with different hydrogen bonds in extracts of *M. azedarach* leaf. The prominent peak at 1689 cm^{-1} confirms the presence of a stretch of C = O of ketones, aldehydes, saturated aliphates and a stretch of α, β unsaturated esters. Furthermore, a peak of 565 cm^{-1} shows the presence of a C–Br stretch of alkyl halides. The obtained peaks are similar to those reported by Zambri et al. [25] and Aisida et al. [28].

The absorption peaks around 3345 and 2854 cm^{-1} in the IR spectrum of the NPs indicate the C-H stretch of alkane and hydroxyl functional group (O–H) of phenol on the

surface of the NPs. The prominent peak around 1689 cm^{-1} indicates the presence of the C = O stretch of aldehydes, saturated aliphates, ketones, and β unsaturated esters. The peak of around 1078 cm^{-1} lies in the C-O stretching vibrations of carboxylic acid, esters, alcohols, and ether domain. The NP spectrum shows a peak at 518 cm^{-1} that corresponds to the Fe–O stretching band of the Fe_3O_4-NPs. The formation of Fe_3O_4-NPs mediated by extracts of *M. azedarach* leaves was confirmed with these properties. Zambri et al. [25] reports a closely related strong peak in the range of 586 cm^{-1}, indicating the presence of Fe_3O_4-NPs for plant extract-mediated nanoparticles. An absorption peak between 400 and 600 cm^{-1} was reported by Bharathi et al. [31], which shows the Fe–O stretch vibrations of iron oxide nanoparticles. The absence of some spectra in the synthesised Fe_3O_4-NPs that appear in the extract may probably mean that the spectra functional groups were used up during the synthesis of the iron oxide nanoparticles, where they acted as reducing and capping agents.

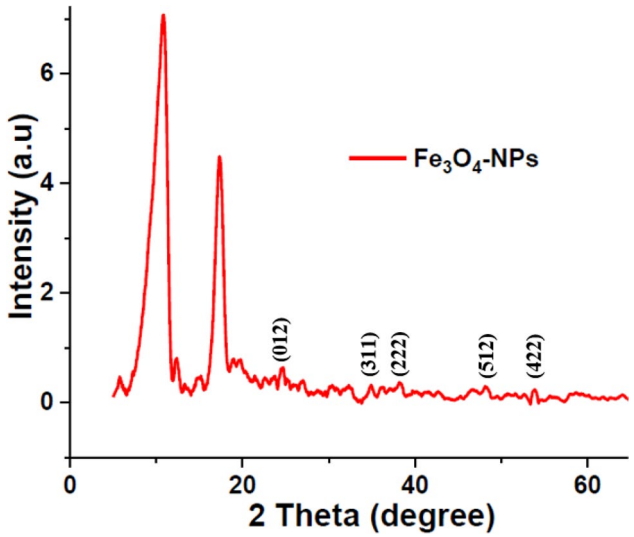

Fig. 5 X-ray diffraction spectrum of the iron oxide nanoparticles mediated via *Melia azedarach* leaves extract

3.6 X-ray Diffraction (XRD) Analysis

The biosynthesised Fe_3O_4-NPs via *Melia azedarach* leaf extracts were analysed using X-ray diffraction technique. This method provide data on purity and crystalline nature of the Fe_3O_4-NPs. Diffraction peaks of 24.6°, 35.6°, 38.4°, 48.2°, and 54.5° were obtained for the synthesised NPs (Fig. 5). The peak values detected in this study correspond to the lattice or crystal plane of (012), (311), (222), (512), and (422) that denotes the crystalline phase of Fe_3O_4-NPs, according to the joint committee on powder diffraction studies standard (JCPDS). Related results were obtained by Kanagasubbulakshmi and Kadirvelu [32], who bio-synthesised iron oxide NPs via *Lagenaria siceraria* leaf extract and reported diffraction peaks at 28.6° and 32.2° that correspond to 220 and 222. Sandhya and Kalaiselvam [33], also reported similar diffraction peaks (29° 35.5°, and 36.8°). From the figure above, the XRD pattern shows both narrow and broad diffraction peaks which indicates that the synthesised. NPs are crystalline in nature [32]. However, the narrow peak detected signifies that the synthesised NPs was crystalline in nature while the broad peak detected indicates that the synthesised NPs were small and fine particles [33].

3.7 Scanning Electron Microscopy (SEM) with Energy Dispersive X-ray (EDX)

Scanning electron imaging with EDX analysis was performed to further confirm the morphology and elemental characteristics of the synthesised NPs. From the SEM images in Fig. 6, the Fe_3O_4-NPs synthesised through *Melia azedarach* leaves extract show an irregularly shaped structure. The EDX analysis of the synthesised NP reveals the presence of 77.23% iron and 22.77% oxygen as the main elemental components (Fig. 7). Other elemental signals

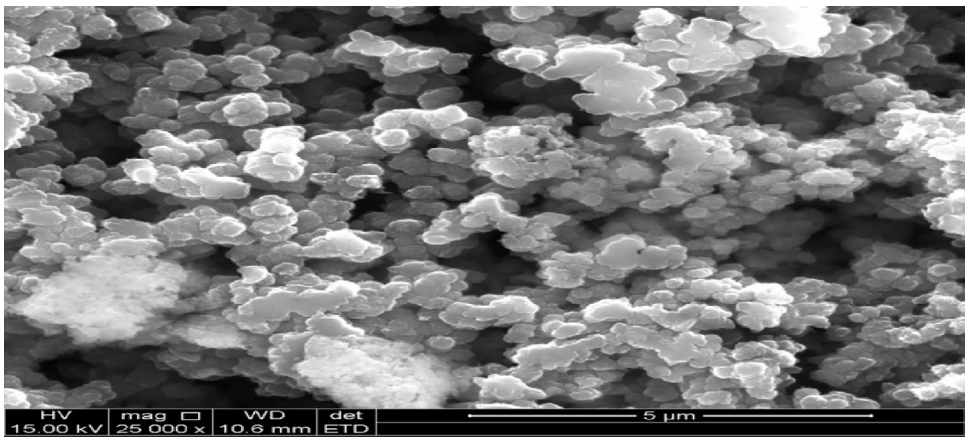

Fig. 6 Scanning electron microscopy image of iron oxide nanoparticles mediated by the extract of *Melia azedarach* leaves

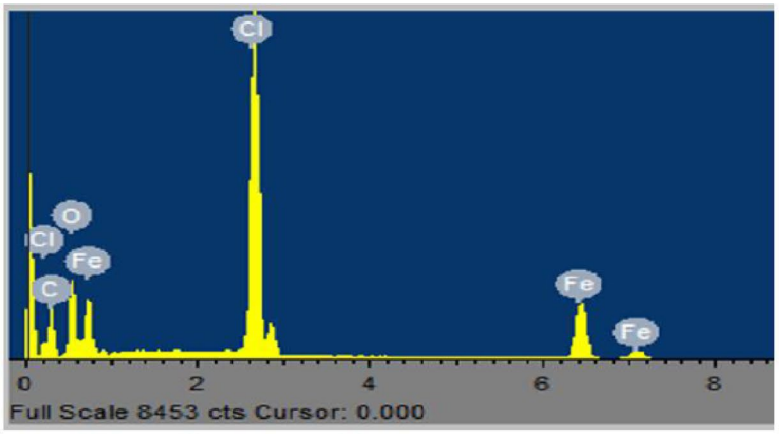

Elemental composition	% Composition
Iron	77.23
Oxygen	22.77

Fig. 7 Energy dispersive X-ray spectrum of iron oxide nanoparticles mediated by extract of *Melia azedarach* leaves

observed such as chlorine (Cl) could have originated from the precursor $FeCl_3.6H_2O$ used in the synthesis process, while the carbon (C) could originated from the plant (*Melia azedarach*), as it is part of the elemental constituents of the plant.

3.8 Transmission Electron Microscopy (TEM)

The TEM micrographs obtained for the plant-derived iron oxide nanoparticles as shown in Fig. 8a were spherical. The average particle size distribution for the obtained particles was determined using the Image J application, where particles were measured at random and represented using a histogram (Fig. 8b). The average particle size for Fe_3O_4-NPs synthesised via the extract of *M. azedarach leaves* was 49.75 nm. The TEM images obtained also indicate the agglomeration of the particles with each other. This can be traced to the occurrence of biological components of *M. azedarach* leaf extract around Fe_3O_4-NPs that result in particles joining together.

3.9 Antimicrobial Activity of the NPs

The outcome of the antimicrobial assay of the NPs tested against diarrhoeal pathogens using the 96-well broth diffusion method and TTC reagent shows that all the isolates tested were susceptible to the synthesised NPs (Fig. 9). The colour of the wells that contain bacteria and TTC without NPs turns red, while the colour of the wells that contain bacteria, TTC, and NPs retains the dark colour of the solution. The MIC of the NPs against diarrhoeal pathogens in this study varied considerably. *V. cholerae* was found to be the most susceptible bacterium to NP, with a MIC of 31 µg/mL, while both *E. coli* and *S. enterica* have a MIC of 62 µg/mL (Fig. 10). The variation in antimicrobial activities of NPs could be explained by several parameters, including size, charge, chemical makeup, and the agglomeration state of NPs [2].

Vibrio cholerae was found to have the lowest MBC value of 250 µg/mL, while *E. coli* and *S. enterica* have the greatest MBC value of 500 µg/mL (Fig. 11). The percentages of *E. coli, V. cholerae,* and *S. enterica* cells killed by NPs after 4 h of contact time were 20, 8, and 8%, respectively. At 8 h, the percentages of *E. coli, V. cholerae,* and *S. enterica* cells killed by NPs were 36, 76, and 36%, respectively. A 100% killing of *V. cholerae* cells was observed at 12 h, compared to 68 and 76% killing of *S. enterica* and *E. coli* cells by the NP, respectively. At the end of 24 h, a 100% killing rate was achieved by NPs against *E. coli, V. cholerae,* and *S. enterica* cells (Fig. 12). Several researchers have reported similar antibacterial activities for Fe_3O_4-NPs [28, 34]. Chauhan and Upadhyay [27] reported the antibacterial activities of iron oxide NPs synthesised from *Lawsonia inermis* (Henna) against *Staphylococcus aureus* and *Staphylococcus typhimurium*. Iron oxide NPs synthesised from *Ulva lactuca* had bactericidal activity against enteric pathogens [34].

The research is still going on to elucidate the actual mode of antimicrobial action by nanoparticles, but studies have suggested that iron oxide nanoparticles exert an antibacterial effect on microorganisms through membrane leakage of intracellular content, DNA damage, and protein damage [2, 35]. Therefore, the antibacterial mode of action of the synthesised Fe_3O_4-NPs could be linked to membrane disruption, DNA damage, and protein damage.

3.10 Cytotoxicity Assay of the Plant-Derived Nanoparticles

In this study, trypan blue assay was employed to evaluate the viability of the HEK293 cells after being treated with the plant derived NPs at different concentrations. After 24 h of incubation, the treated cell lines were still

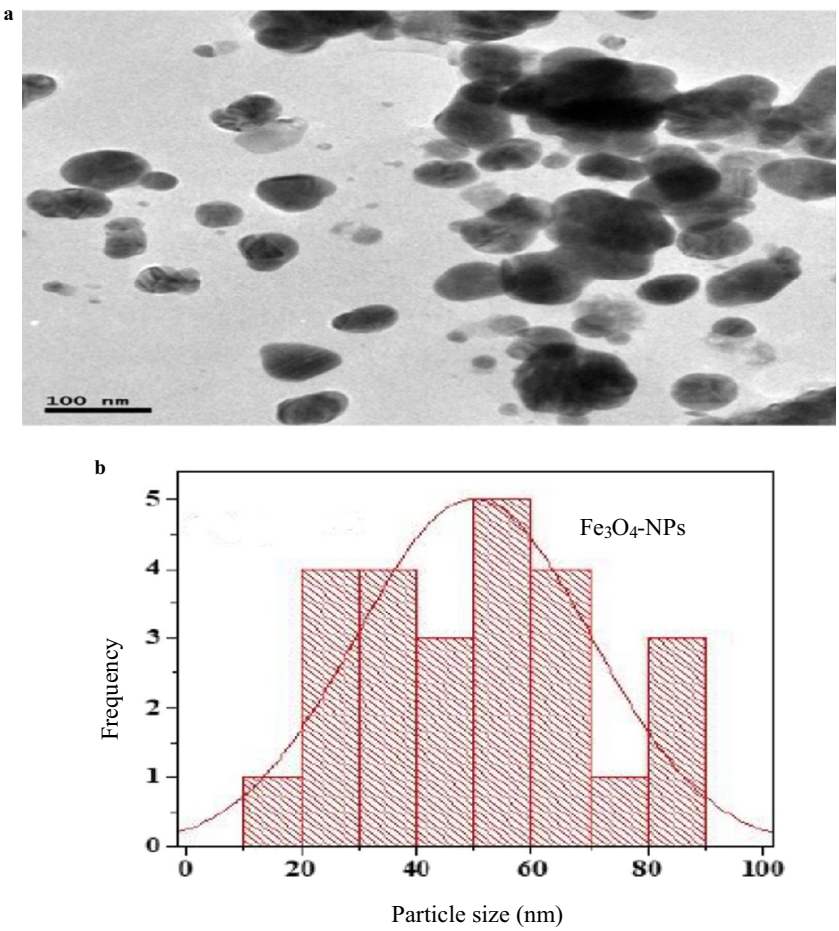

Fig. 8 **a**Transmission electron microscopy image of the iron oxide nanoparticles mediated by *Melia azedarach* leaf extract. **b** A histogram illustrating the corresponding particle sizes of the iron oxide nanoparticles mediated via *Melia azedarach* leaf extract

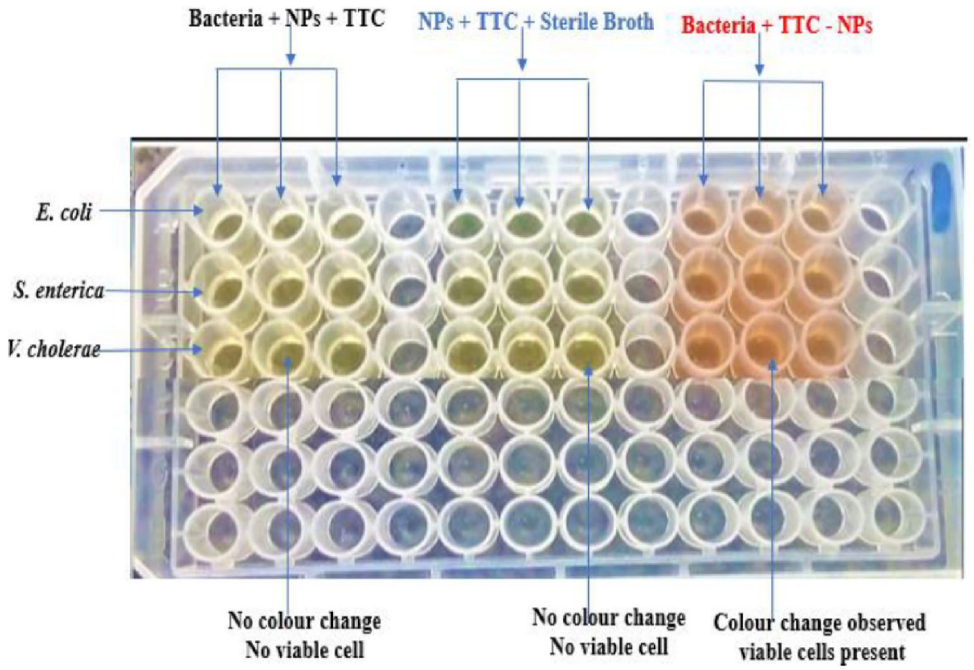

Fig. 9 Antibacterial activity of the nanoparticles against *Escherichia coli, Vibrio cholerae,* and *Salmonella enterica*

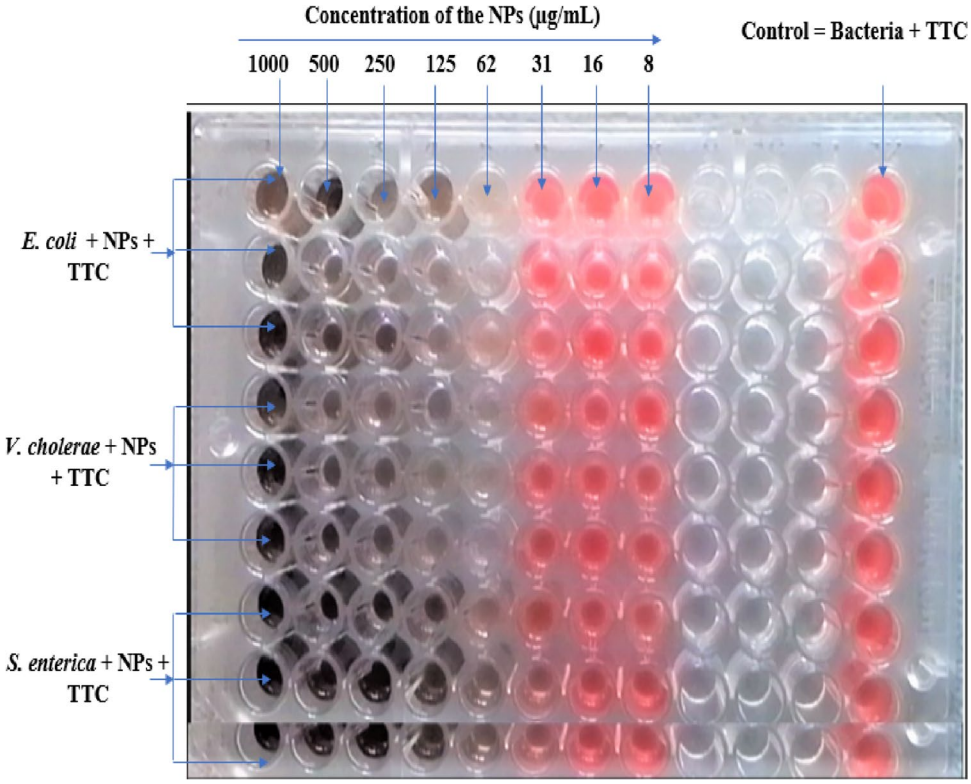

Fig. 10 Minimum inhibitory concentration of the nanoparticles against *Escherichia coli, Vibrio cholerae,* and *Salmonella enterica*

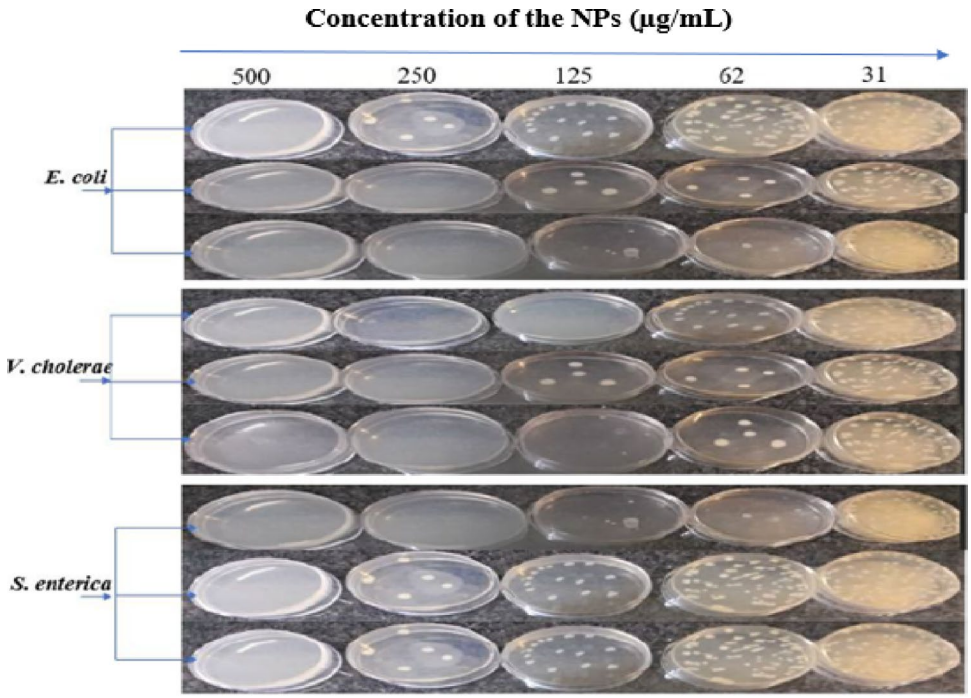

Fig. 11 Minimum bactericidal concentration of nanoparticles against *Escherichia coli, Vibrio cholerae,* and *Salmonella enterica*

viable, with variations in their numbers based on NPs concentration (Fig. 13). In reference to the viable cell count of the control, the cell lines treated with NPs at low concentrations (8, 16, and 32 µg/mL) show 100% viability after 24 h of incubation. The decrease in cell viability at the concentration of 62 µg/mL of the NPs was less than 10%. At 125 µg/mL of NPs, there was 46% decrease in cell viability. It might be concluded that the cytotoxicity of the NPs in this study against HEK293 cell lines was concentration dependent. Several studies have

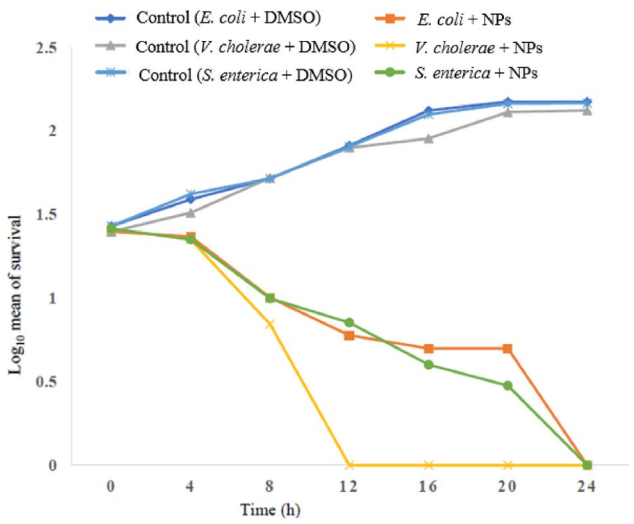

Fig. 12 The rate of killing *Escherichia coli*, *Vibrio cholerae*, and *Salmonella enterica* exhibited by the nanoparticles

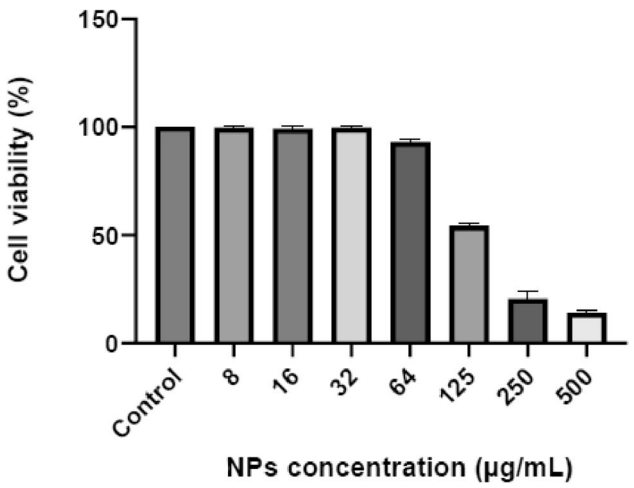

Fig. 13 Cytotoxicity of the nanoparticles against human embryonic kidney 293 cell lines. The error bars indicate the standard deviation

reported that Fe_3O_4-NPs synthesised from plant extract at concentrations less than 100 µg/mL did not exhibit cytotoxicity to tested cells and did not induce any changes in cellular morphology [36, 37]. Pillai et al. [37] evaluated the toxicity of biosynthesised Fe_3O_4-NPs and proposed that Fe_3O_4-NPs did not present a significant impact on cell viability at low concentrations. Furthermore, Temelie et al. [36] reported that green synthesised Fe_3O_4-NPs at low concentrations were not toxic to normal cells. The cytotoxicity data of the NPs against the HEK293 cell lines has been presented in Fig. 13.

4 Conclusion

This study reports the synthesis of NPs mediated by the extract of *M. azedarach* and their antibacterial properties. The synthesised NPs were rapid and not expensive. The *M. azedarach* extract contained phytochemicals that include flavonoids and phenols that serve as reducing, capping, and stabilising agents. Furthermore, the synthesised NPs showed potent antibacterial activities against multidrug-resistant *E. coli, V. cholerae,* and *S. enterica* tested. Additionally, the synthesised NPs showed a short killing rate against *E. coli, V. cholerae,* and *S. enterica* tested. Interestingly, the concentrations of the NPs required to inhibit the growth of *E. coli*, *V. cholerae,* and *S. enterica* were not toxic to HEK293 cells. These NPs may be useful in therapeutic applications aimed at combating pathogens.

Acknowledgements The authors wish to appreciate the Department of Microbiology, School of Biological Sciences, North-West University, Mafikeng, South Africa.

Author Contribution CA, AA, OF and TA: conceptualization and resources. TA, DA, BO, JF, KM, and CA: writing and editing. TA: Experimenting. CA, AA, and OF: supervision. All authors contributed to the article and approved the submitted version.

Funding Open access funding provided by North-West University. We are grateful to the North-West University and the Department of Microbiology, School of Biological Sciences for the financial support.

Data Availability The datasets used and/or analysed during the current study are available from the corresponding author on reasonable request.

Declarations

Competing interests The authors declare no competing interests.

Ethics Approval The ethics clearance for the study was collected from the North-West University (NWU) AnimCare Committee, and an ethics number of NWU-00771–23-A5 was assigned to this study.

Consent for Publication All authors contributed to the article and approved the submitted version for the publication.

Research Involving Humans and Animals Statement None.

Conflict of Interest The authors declare no competing interests.

References

1. Shankar, S., & Rosenbaum, J. (2020). Chronic diarrhoea in children: A practical algorithm-based approach. *Journal of Paediatrics Child Health, 56*(7), 1029–1038. https://doi.org/10.1111/jpc.14986
2. Abolarinwa, T. O., Ajose, D. J., Oluwarinde, B. O., Fri, J., Montso, K. P., Fayemi, O. E., et al. (2022). Plant-derived nanoparticles as alternative therapy against diarrheal pathogens in the era of antimicrobial resistance: A review. *Frontiers in Microbiology, 13*, 1007115. https://doi.org/10.3389/fmicb.2022.1007115
3. Vos, T., Lim, S. S., Abbafati, C., Abbas, K. M., Abbasi, M., Abbasifard, M., et al. (2020). Global burden of 369 diseases and injuries in 204 countries and territories, 1990–2019: A systematic analysis for the Global Burden of Disease Study 2019. *The Lancet, 396*(10258), 1204–1222. https://doi.org/10.1016/S0140-6736(20)30925-9
4. Yang, S., Liu, Y., Yang, N., Lan, Y., Lan, W., Feng, J., et al. (2022). The gut microbiome and antibiotic resistome of chronic diarrhea rhesus macaques (Macaca mulatta) and its similarity to the human gut microbiome. *Microbiome, 10*(1), 29. https://doi.org/10.1186/s40168-021-01218-3
5. Mullish, B. H., & Williams, H. R. J. C. M. (2018). Clostridium difficile infection and antibiotic-associated diarrhoea. *Clinical Medicine, 18*(3), 237. https://doi.org/10.7861/clinmedicine.18-3-237
6. Wong, C. S., Jelacic, S., Habeeb, R. L., Watkins, S. L., & Tarr, P. I. (2000). The risk of the hemolytic–uremic syndrome after antibiotic treatment of *Escherichia coli* O157:H7 Infections. *New England Journal of Medicine, 342*(26), 1930–1936. https://doi.org/10.1056/nejm200006293422601
7. Tarr, P. I., & Freedman, S. B. (2022). Why antibiotics should not be used to treat Shiga toxin-producing *Escherichia coli* infections. *Current Opinion in Gastroenterology, 38*(1), 30–38. https://doi.org/10.1097/MOG.0000000000000798
8. Hwang, S.-B., Chelliah, R., Kang, J. E., Rubab, M., Banan-MwineDaliri, E., Elahi, F., et al. (2021). Role of recent therapeutic applications and the infection strategies of Shiga toxin-producing *Escherichia coli*. *Frontiers in Cellular Infection Microbiology, 11*, 450. https://doi.org/10.3389/fcimb.2021.614963
9. Ramstad, S. N., Taxt, A. M., Naseer, U., Wasteson, Y., Bjørnholt, J. V., & Brandal, L. T. J. M. P. (2021). Effects of antimicrobials on Shiga toxin production in high-virulent Shiga toxin-producing *Escherichia coli*. *Microbial Pathogenesis, 152*, 104636. https://doi.org/10.1016/j.micpath.2020.104636
10. Behera, D. K., & Mishra, S. (2022). The burden of diarrhea, etiologies, and risk factors in India from 1990 to 2019: Evidence from the global burden of disease study. *BMC Public Health, 22*(1), 92. https://doi.org/10.1186/s12889-022-12515-3
11. Saravanan, A., Maruthapandi, M., Das, P., Luong, J. H. T., & Gedanken, A. (2021). Green synthesis of multifunctional carbon dots with antibacterial activities. *Nanomaterials, 11*(2), 369. https://doi.org/10.3390/nano11020369
12. Priyadarsini, S., Mukherjee, S., & Mishra, M. (2018). Nanoparticles used in dentistry: A review. *Journal of Oral Biology and Craniofacial Research, 8*(1), 58–67. https://doi.org/10.1016/j.jobcr.2017.12.004
13. Banerjee, S., Vishakha, K., Das, S., Sangma, P. D., Mondal, S., Ganguli, A. J. W. J., o. M., et al. (2022). Oxidative stress, DNA, and membranes targets as modes of antibacterial and antibiofilm activity of facile synthesized biocompatible keratin-copper nanoparticles against multidrug resistant uro-pathogens. *World Journal of Microbiology Biotechnology, 38*(2), 1–16. https://doi.org/10.1007/s11274-021-03187-z
14. Korani, M., Ghazizadeh, E., Korani, S., Hami, Z., & Mohammadi-Bardbori., A. (2015). Effects of silver nanoparticles on human health. *European Journal of Nanomedicine, 7*(1), 51–62. https://doi.org/10.1515/ejnm-2014-0032
15. Zoroddu, M. A., Aaseth, J., Crisponi, G., Medici, S., Peana, M., & Nurchi, V. M. (2019). The essential metals for humans: A brief overview. *Journal of Inorganic Biochemistry, 195*, 120–129. https://doi.org/10.1016/j.jinorgbio.2019.03.013
16. Patel, J. K., Patel, A., and Bhatia, D. Introduction to nanomaterials and nanotechnology. In: Patel JK, Pathak YV, editors. Emerging Technologies for Nanoparticle Manufacturing: Springer International Publishing 2021 3–23
17. Modan, E. M. and Plaiasu, A. G. 2020. Advantages and disadvantages of chemical methods in the elaboration of nanomaterials The Annals of "Dunarea de Jos" University of Galati Fascicle IX, Metallurgy and Materials Science 43 1 53 60 https://doi.org/10.35219/mms.2020.1.08
18. Karpagavinayagam, P., & Vedhi, C. (2019). Green synthesis of iron oxide nanoparticles using Avicennia marina flower extract. *Vacuum, 160*, 286–292. https://doi.org/10.1016/j.vacuum.2018.11.043
19. Khan, S. A., Shahid, S., & Lee, C.-S.J.B. (2020). Green synthesis of gold and silver nanoparticles using leaf extract of clerodendrum inerme; characterization, antimicrobial, and antioxidant activities. *Biomolecules, 10*(6), 835. https://doi.org/10.3390/biom10060835
20. Jadoun, S., Arif, R., Jangid, N. K., & Meena, R. K. (2021). Green synthesis of nanoparticles using plant extracts: A review. *Environmental Chemistry Letters, 19*(1), 355–374. https://doi.org/10.1007/s10311-020-01074-x
21. Chinnasamy, G., Chandrasekharan, S., & Bhatnagar, S. (2019). Biosynthesis of silver nanoparticles from Melia azedarach: Enhancement of antibacterial, wound healing, antidiabetic and antioxidant activities. *International Journal of Nanomedicine, 14*, 9823–9836. https://doi.org/10.2147/ijn.S231340
22. Humphries, R., Bobenchik, A. M., Hindler, J. A., & Schuetz, A. N. (2021). Overview of changes to the clinical and laboratory standards institute performance standards for antimicrobial susceptibility testing. *Journal of Clinical Microbiology, 59*(12), 10–1128. https://doi.org/10.1128/jcm.00213-21
23. Shubham, S., Mishra, R., Gautam, N., Nepal, M., Kashyap, N., & Dutta, K. (2019). Phytochemical analysis of papaya leaf extract: Screening test. *EC Dental Science, 18*(3), 485–490.
24. Madubuonu, N., Aisida, S. O., Ali, A., Ahmad, I., Zhao, T. K., Botha, S., Maaza, M., & Ezema, F. I. (2019). Biosynthesis of iron oxide nanoparticles via a composite of Psidium guavaja-Moringa oleifera and their antibacterial and photocatalytic study. *Journal of Photochemistry and Photobiology B: Biology, 199*, 111601. https://doi.org/10.1016/j.jphotobiol.2019.111601
25. Zambri, N. D. S., Taib, N. I., Abdul Latif, F., & Mohamed, Z. (2019). Utilization of neem leaf extract on biosynthesis of iron oxide nanoparticles. *Molecules, 24*(20), 3803. https://doi.org/10.3390/molecules24203803
26. Ahmed, A., Pelton, M., & Guest, J. R. (2017). Understanding how acoustic vibrations modulate the optical response of plasmonic metal nanoparticles. *ACS Nano, 11*(9), 9360–9369. https://doi.org/10.1021/acsnano.7b04789
27. Chauhan, S., & Upadhyay, L. S. B. (2019). Biosynthesis of iron oxide nanoparticles using plant derivatives of Lawsonia inermis (Henna) and its surface modification for biomedical application. *Nanotechnology for Environmental Engineering, 4*(1), 8. https://doi.org/10.1007/s41204-019-0055-5
28. Aisida, S. O., Madubuonu, N., Alnasir, M. H., Ahmad, I., Botha, S., Maaza, M., et al. (2020). Biogenic synthesis of iron oxide nanorods using Moringa oleifera leaf extract for antibacterial applications. *Applied Nanoscience, 10*(1), 305–315. https://doi.org/10.1007/s13204-019-01099-x

29. Neupane, B. P., Chaudhary, D., Paudel, S., Timsina, S., Chapagain, B., Jamarkattel, N., et al. (2019). Himalayan honey loaded iron oxide nanoparticles: Synthesis, characterization and study of antioxidant and antimicrobial activities. *International Journal of Nanomedicine, 14*, 3533–3541. https://doi.org/10.2147/ijn.S196671
30. Rahman, S. S. U., Qureshi, M. T., Sultana, K., Rehman, W., Khan, M. Y., Asif, M. H., et al. (2017). Single step growth of iron oxide nanoparticles and their use as glucose biosensor. *Results in Physics, 7*, 4451–4456. https://doi.org/10.1016/j.rinp.2017.11.001
31. Bharathi, D., Preethi, S., Abarna, K., Nithyasri, M., Kishore, P., & Deepika, K. (2020). Bio-inspired synthesis of flower shaped iron oxide nanoparticles (FeONPs) using phytochemicals of Solanum lycopersicum leaf extract for biomedical applications. *Biocatalysis and Agricultural Biotechnology, 27*, 101698. https://doi.org/10.1016/j.bcab.2020.101698
32. Kanagasubbulakshmi, S., & Kadirvelu, K. (2017). Green synthesis of iron oxide nanoparticles using Lagenaria siceraria and evaluation of its antimicrobial activity. *Defence Life Science Journal, 2*(4), 422–427. https://doi.org/10.14429/dlsj.2.12277
33. Sandhya, J., & Kalaiselvam, S. (2020). Biogenic synthesis of magnetic iron oxide nanoparticles using inedible borassus flabellifer seed coat: Characterization, antimicrobial, antioxidant activity and in vitro cytotoxicity analysis. *Materials Research Express, 7*(1), 015045. https://doi.org/10.1088/2053-1591/ab6642
34. Bensy, A. D., Christobel, G. J., Muthusamy, K., & Alfarhan, A. (2022). Green synthesis of iron nanoparticles from *Ulva lactuca* and bactericidal activity against enteropathogens. *Journal of King Saud University-Science, 34*(3), 101888. https://doi.org/10.1016/j.jksus.2022.101888
35. Ajose, D. J., Abolarinwa, T. O., Oluwarinde, B. O., Montso, P. K., Fayemi, O. E., Aremu, A. O., et al. (2022). Application of plant-derived nanoparticles (PDNP) in food-producing animals as a bio-control agent against antimicrobial-resistant pathogens. *Biomedicines, 10*(10), 2426. https://doi.org/10.3390/biomedicines10102426
36. Temelie, M., Popescu, R., Cocioaba, D., Vasile, B., & Savu, D. (2018). Biocompatibility study of magnetite nanoparticle synthesized using a green method. *Romanian Journal of Physics, 63*, 703.
37. Pillai, R. R., Sreelekshmi, P. B., Meera, A. P., & Thomas, S. (2022). Biosynthesized iron oxide nanoparticles: Cytotoxic evaluation against human colorectal cancer cell lines. *Materials Today: Proceedings, 50*, 187–195. https://doi.org/10.1016/j.matpr.2022.01.151